人工脏器

人工脏器是指：通过人工制造出适应于人体的器官以代替机能不全的脏器。

混合型人工肝脏的模式图

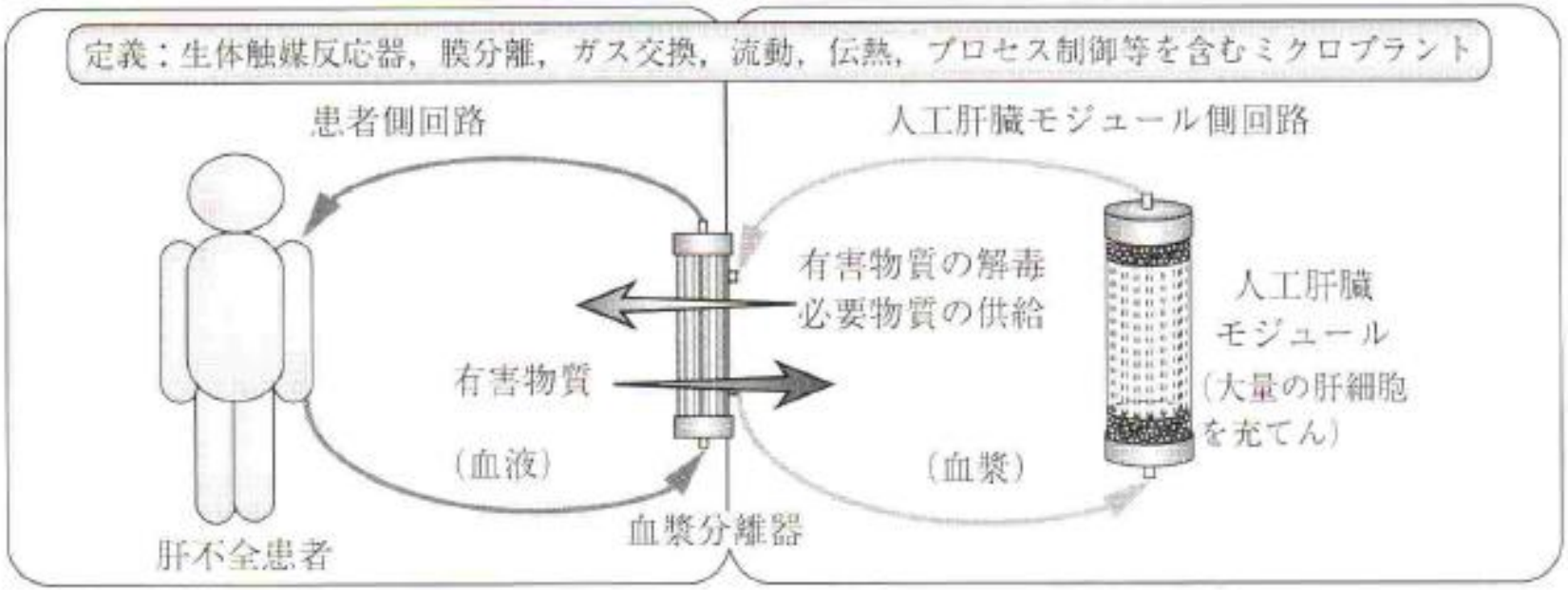

図 6.15　ハイブリッド型人工肝臓の基本概念

第8次讲义

资料来源：
Artificial Kidney ， by Dayong Gao
Introduction to Heat Transfer，
By Incropera, FP

人体肾脏结构

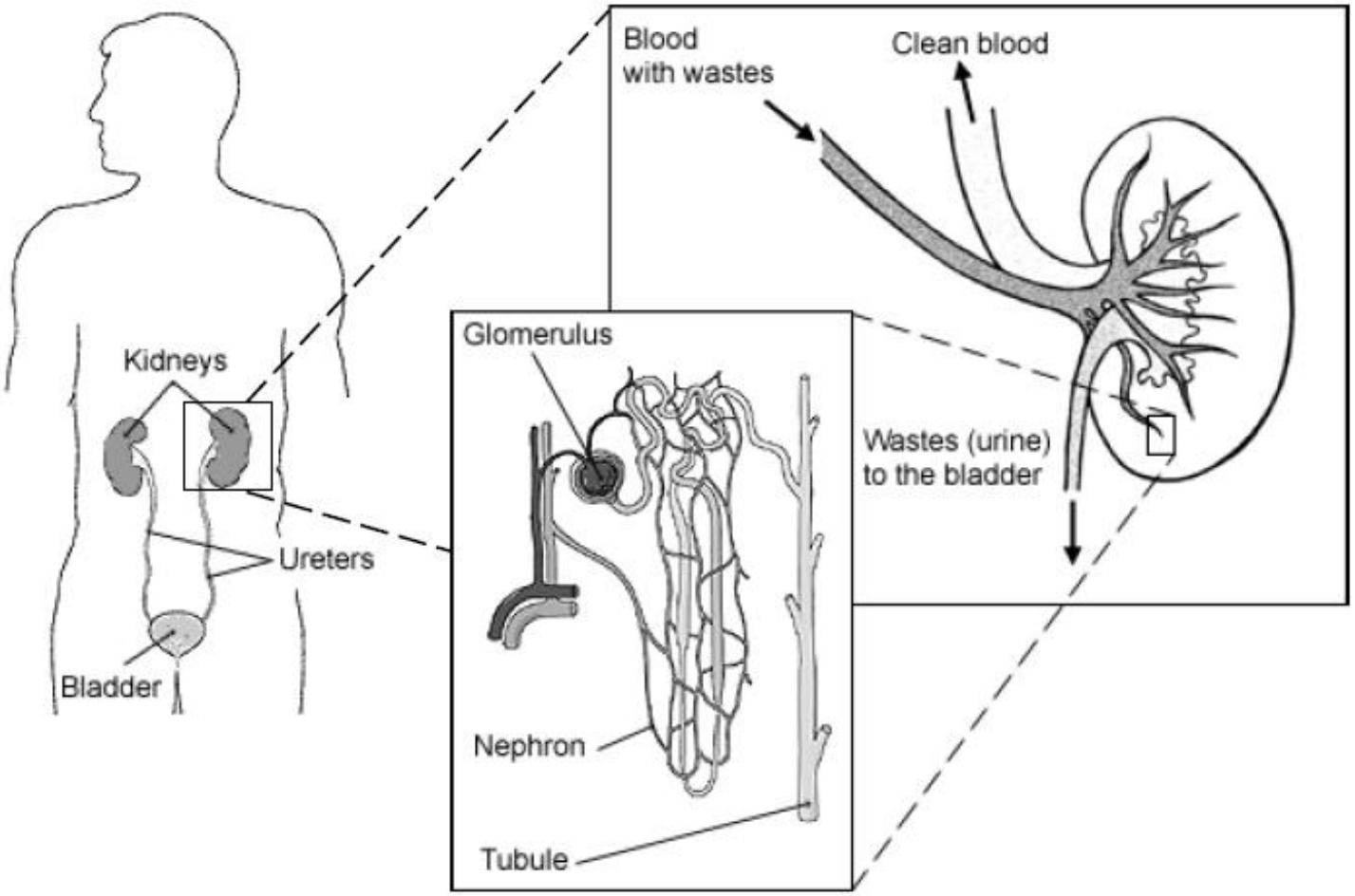
Kidneys
Ureters
Bladder
Blood
with wastes
Clean blood
Wastes (urine)
to the bladder
Glomerulus
Nephron
Tubule

renal corpuscle

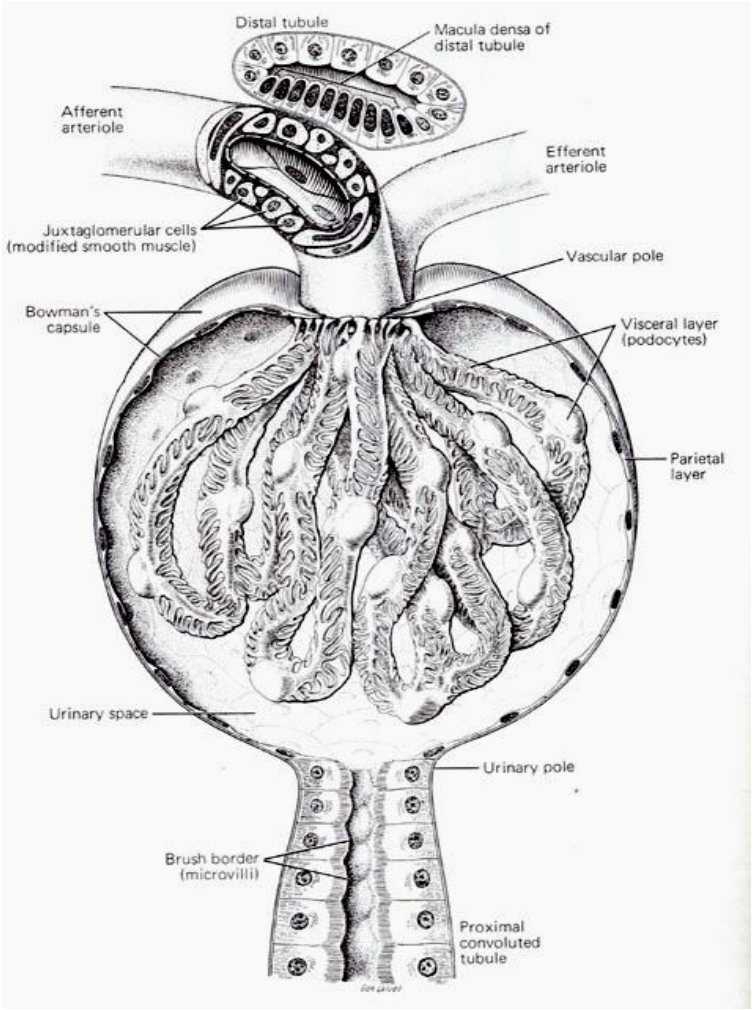

podocyte

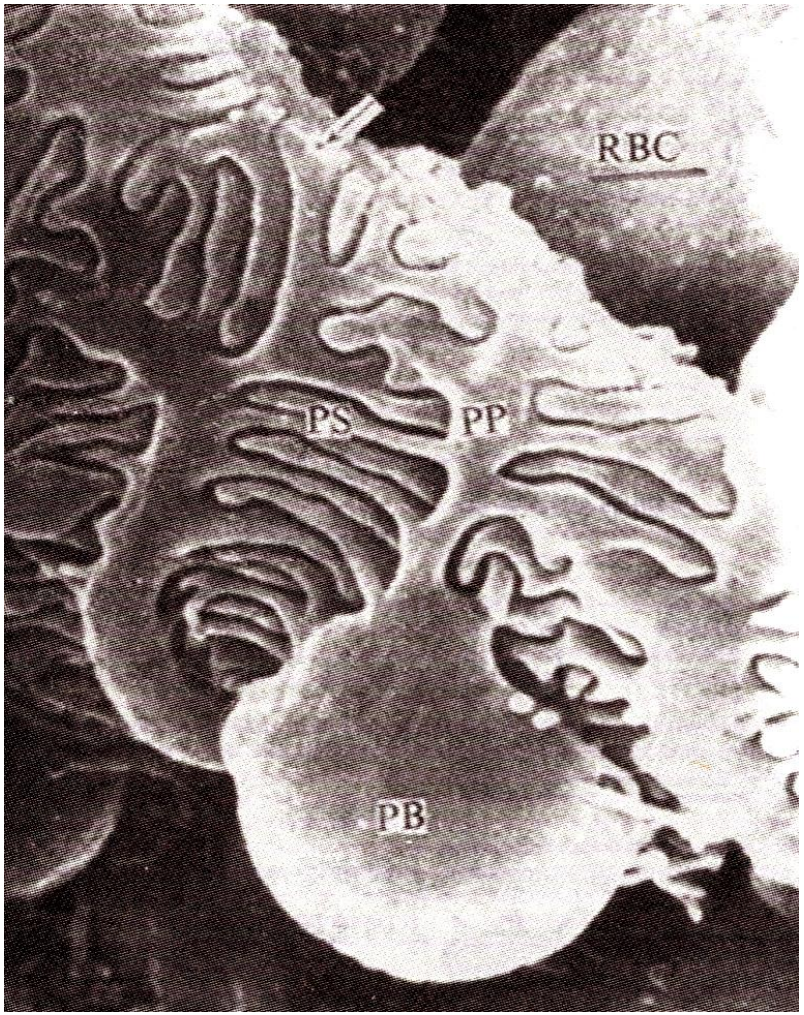

filtration barrier

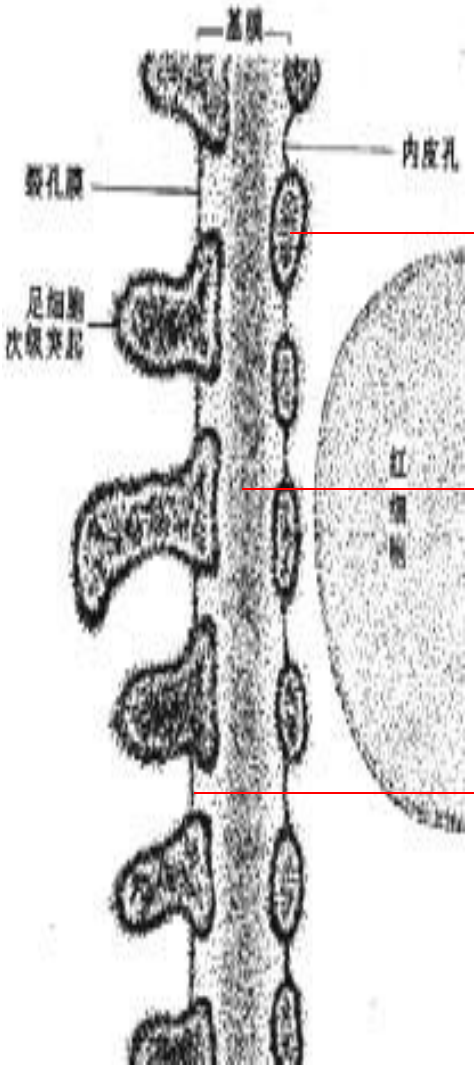

endothelium of fenestrated capillary

basement membrane

slit membrane of podocyte

肾衰竭患病人数的推移和预测（美国）

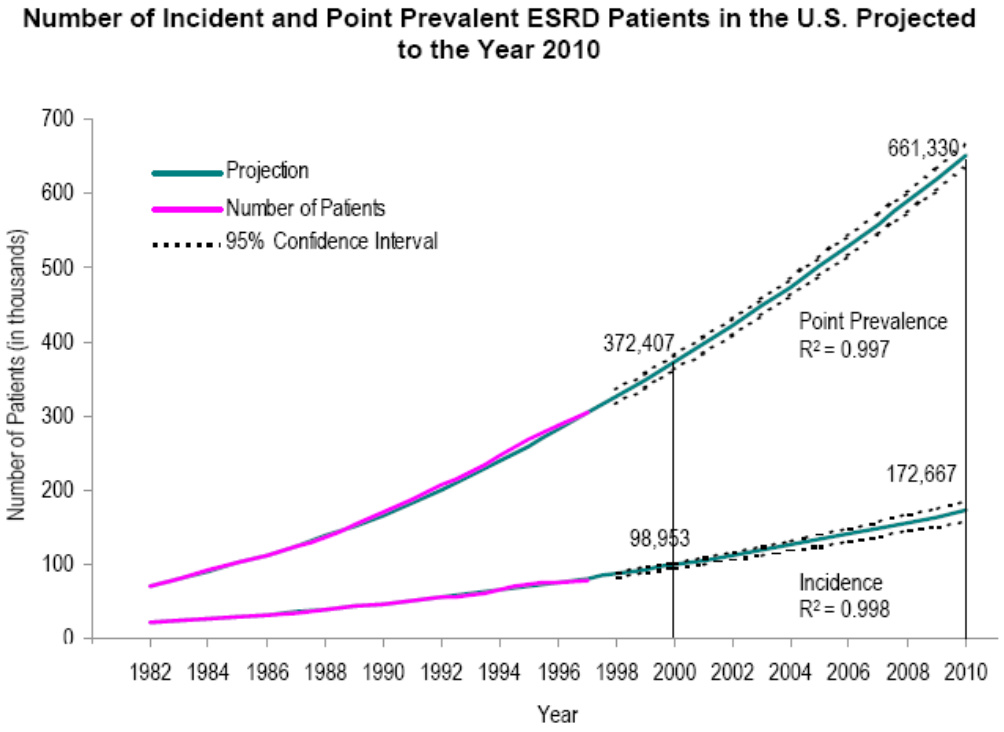

Figure 1.2 Number of reported incident and point prevalent end-stage renal disease (ESRD) patients in the U.S. projected to the year 2010. These graphs are plotted using forecasting and time-series analyses, with stepwise autoregressive models for incidence and exponential smoothing models for prevalence. The projections are determined using data from the year 1982 to 1997. Incidence is the number of people in a population newly diagnosed with the disease in a given year, and point prevalence is the number of people in a population who have the disease on December 31st in a given year. ESRD patients who died before receiving treatment or whose therapy is not reported to the Health Care Financing Administration (HCFA) are not included in these data (Data Source: USRDS 2000 Annual Data Report).

治疗肾衰竭所需医疗费的推移和预测 （美国）

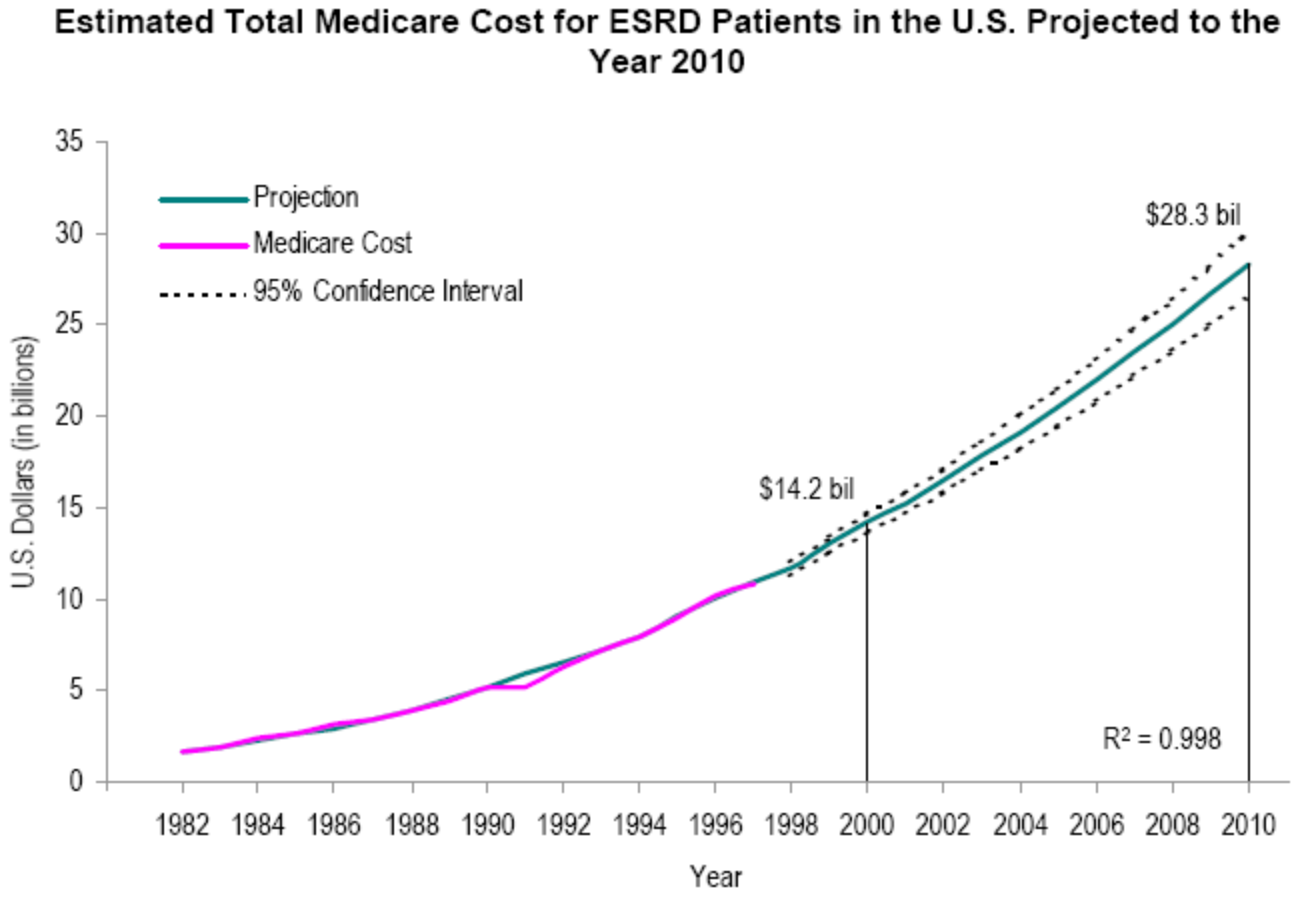

Figure 1.5 Estimated total Medicare cost for end-stage renal disease (ESRD) patients in the U.S. projected to the year 2010. These graphs are plotted using forecasting and time-series analyses with stepwise autoregressive models. The projections are determined using data from the year 1982 to 1997 (Data Source: USRDS 2000 Annual Data Report (USRDS 2000)).

世界各国肾衰竭（ESRD）的患病人数推移

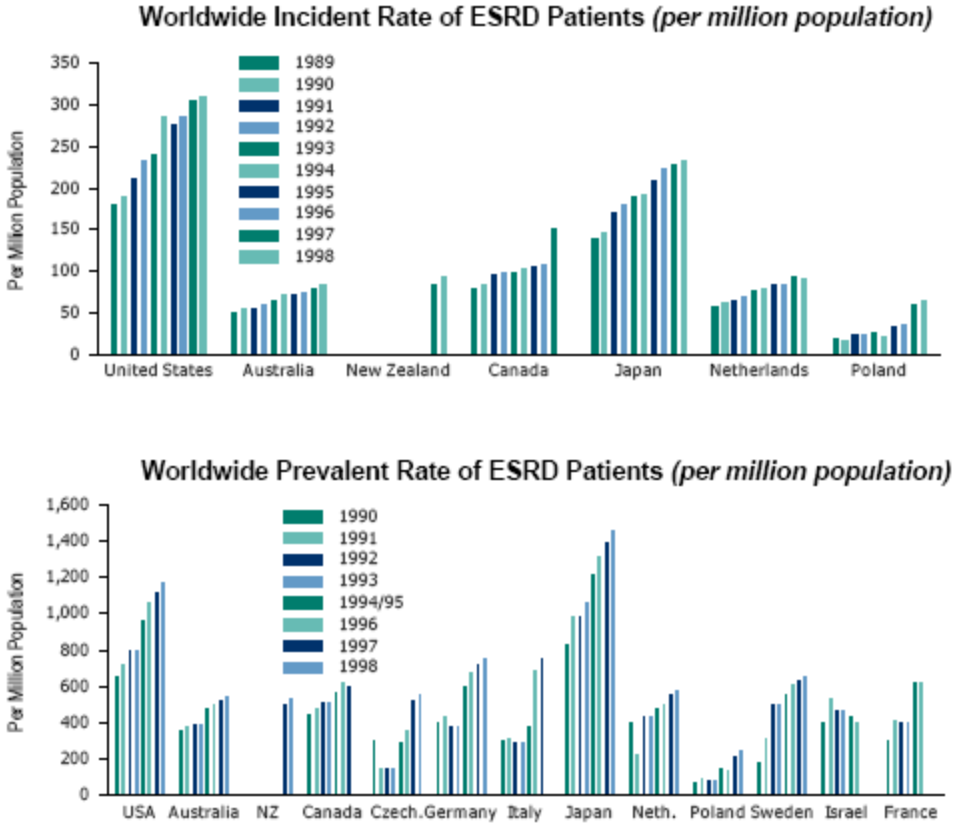

Figure 1.6 Reported worldwide incident and prevalent rates of end-stage renal disease (ESRD) patients. Incident rate is the reported rate of people in a country newly diagnosed with the disease in a given year, and prevalent rate is the reported rate of people in a country who have the disease in a given year In the incident rates, data for Japan include dialysis patients only. In the prevalent rates, 1995 data are listed for the U.S. and Australia, and 1994 data are listed for all other countries. The data presented here account only for a small portion of the information available from individual countries (Data Source: USRDS 2000 Annual Data Report).

不同治疗方式下ESRD患者第一年的死亡率变化

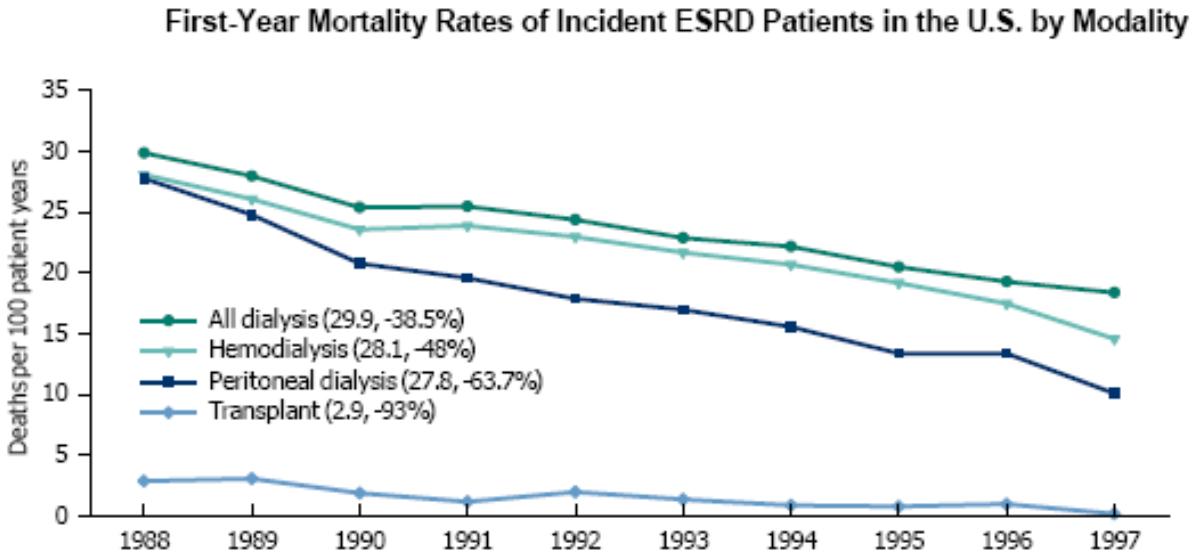

Figure 1.7 First-year mortality rates of incident end-stage renal disease patients in the U.S. by modality. The first-year mortality rates in each modality were determined by using the average of incident patients in the year 1997 in each modality as the reference population, and were adjusted for age, gender, race and primary diagnosis of diabetes. The number of deaths per 100 patient-years in the year 1988, and the percent change of the values from the year 1988 to 1997 by modality are shown in the legend (Data Source: USRDS 2000 Annual Data Report).

不同治疗方式下ESRD患者生存率的变化

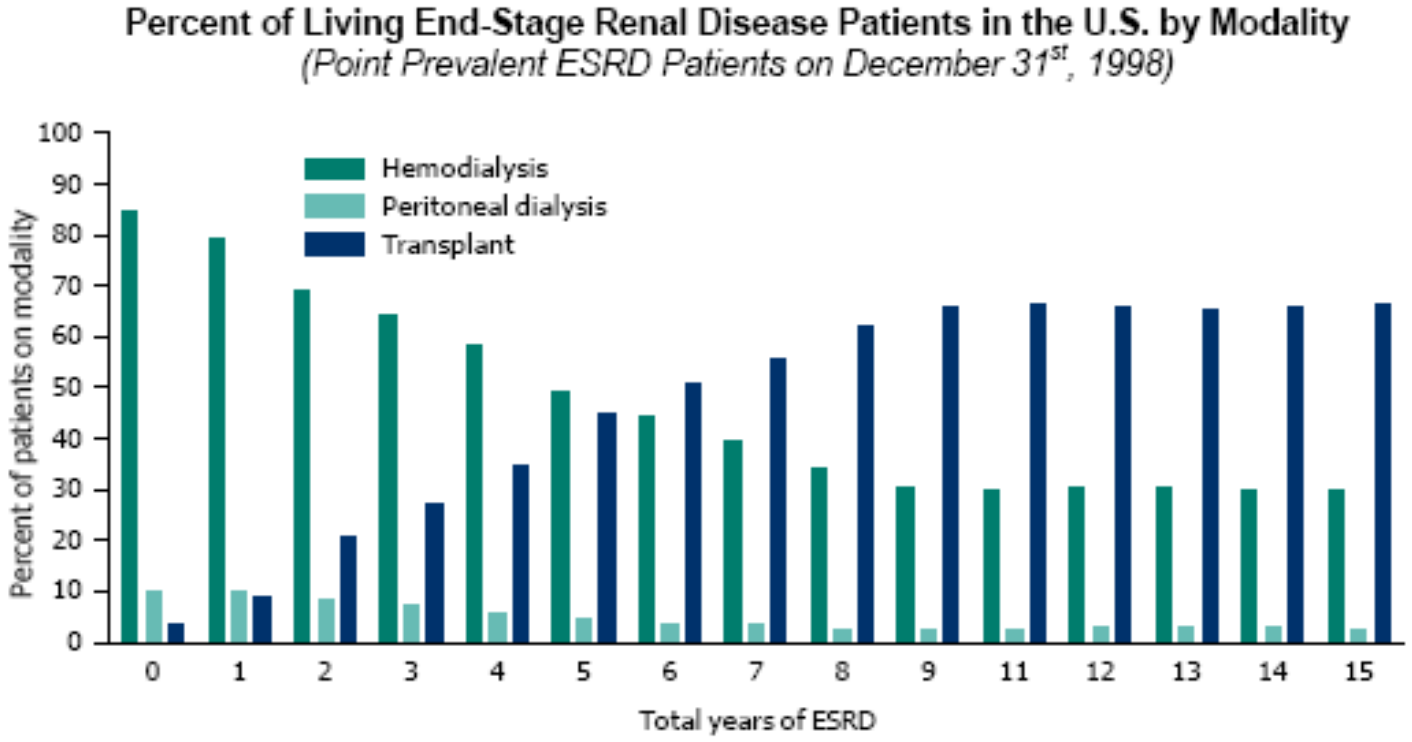

Figure 1.8 The percent of point prevalent end-stage renal disease patients in the U.S. by modality on December 31st, 1998. (Data Source: USRDS 2000 Annual Data Report).

人工肾的外形尺寸及结构

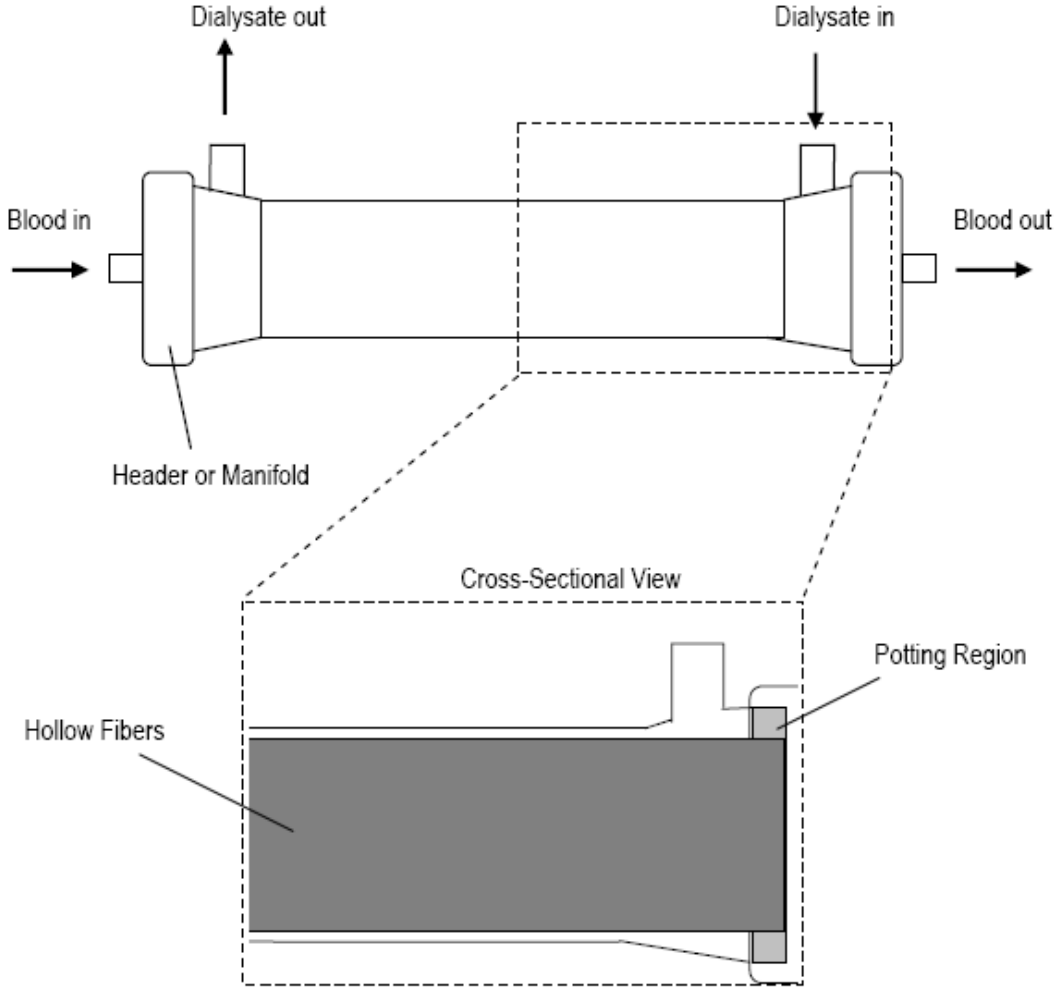

Figure 2.1 A general schematic diagram of an artificial kidney
(The shape of an artificial kidney varies slightly from different manufacturers)

人工肾的结构和机能

- 逆流传质装置，类似于列管式热交换器：shell and tube heat exchanger
- 根据人工肾的大小，装置中有6000-12000个中空纤维，中空纤维的孔径为200 μm，壁厚15-50 μm
- 中空纤维部分：通过血液；外壳部分：通过透析液（dialysis liquid)

逆流换热器的结构

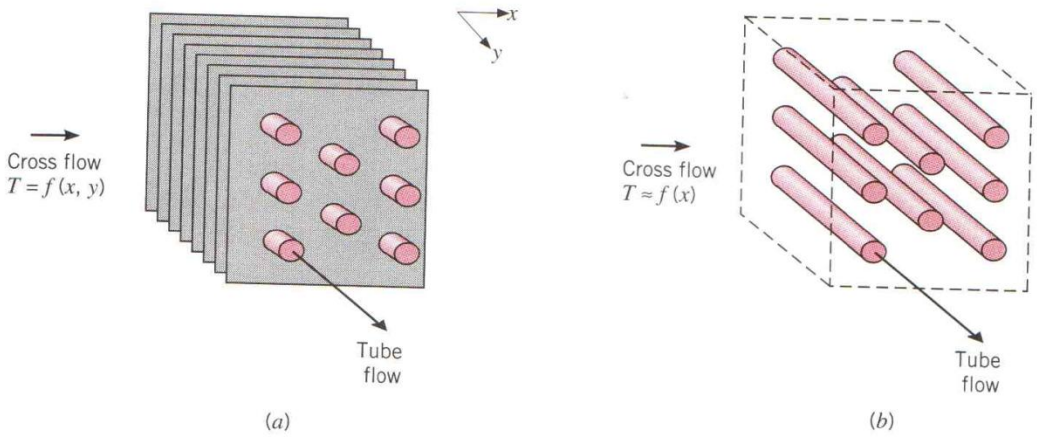

FIGURE 11.2 Cross-flow heat exchangers. (*a*) Finned with both fluids unmixed. (*b*) Unfinned with one fluid mixed and the other unmixed.

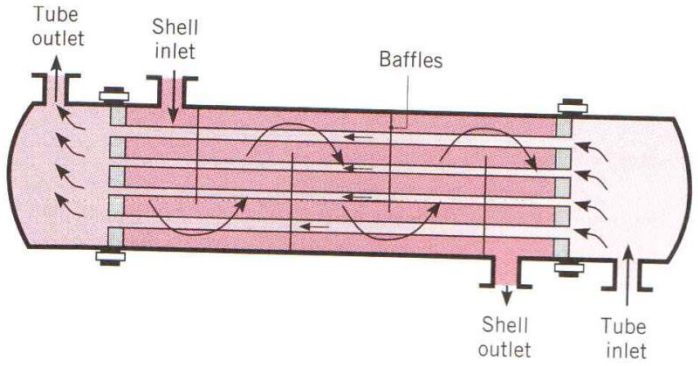

FIGURE 11.3 Shell-and-tube heat exchanger with one shell pass and one tube pass (cross-counterflow mode of operation).

中空纤维的作用
半通透膜：在血液和透析液之间起着半通透的屏蔽作用
中空纤维的优点：
使单位体积的表面积最大化
理想的人工肾：血液和透析液全部通过中空纤维的内外侧，使传质过程最优化
传质效率降低的情形：
中空纤维管束空间配置不合适-影响了透析液通过而发生堵塞
中空纤维内的孔隙发生堵塞而使血液的过滤不通畅

中空纤维的横断面及内表面

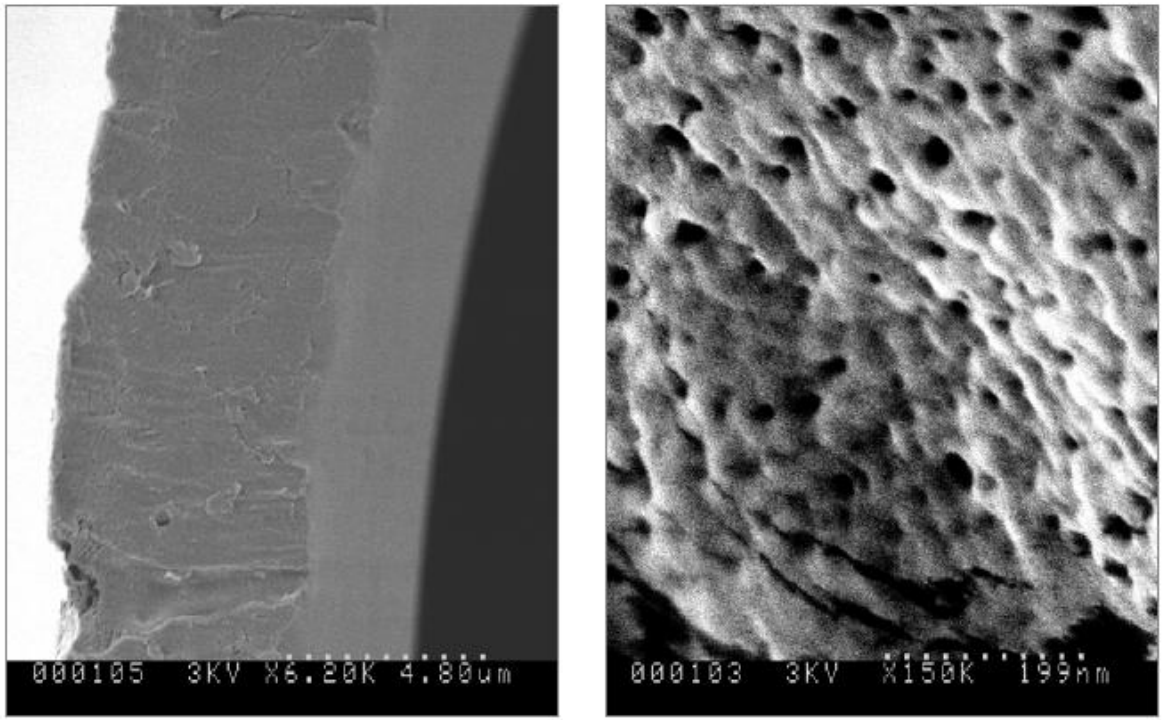

(a)

Figure 2.2 The scanning electron micrographs of a CT190G hollow fiber. (a) Cross-sectional view at 6200X and (b) inner surface view at 150,000X of the hollow fiber. The CT190G hollow fiber is made of cellulose triacetate.

透析膜：dialysis membrane

理想的透析膜:
能够象人体肾一样清除各样尿毒溶质
不会与血液以及药物发生逆向反应
可以经受不同的运行环境

透析膜的种类:
纤维质透析膜 (cellulosic membrane)
合成膜 (synthetic membrane)

三种不同规格透析装置的参数

三醋酯纤维

聚醚砜

Table 2.1 Physical characteristics of different clinical dialyzers

	CT190G (Baxter)	Polyflux 17S (Gambro)	SYNTRA160 (Baxter)
Membrane Material	Cellulose Triacetate	Polyamide S™ [1]	DIAPES® [2]
Effective Membrane Area (m^2)	1.9	1.7	1.6
Fiber Inner Diameter (µm)	200	215	200
Fiber Wall Thickness (µm)	15	50	30
Nominal Fiber Number	12,000	10,000	11,200
Fiber Packing Density[3] (Fibers per cm^2)	1116	722	891[4]
Ultrafiltration Coefficient[5] (mL/hr/mmHg)	36	71	84
Multifilament Spacer Yarns	No	No	Yes

All data were obtained from the manufacturer literature (specification data sheets), unless noted otherwise.

[1] Polyamide S™ = Polyarylethersulfone

[2] DIAPES® = Polyethersulfone

[3] Measured and determined in the laboratory.

[4] Did not take into account the multifilament spacer yarns.

[5] Ultrafiltration coefficients were determined in vitro with bovine blood (HCT = 32%, Temp = 37°C). HCT = Hematocrit

中空纤维断面结构

独特的空隙结构：外层，中间支持层，手指型结构层，微区域内层

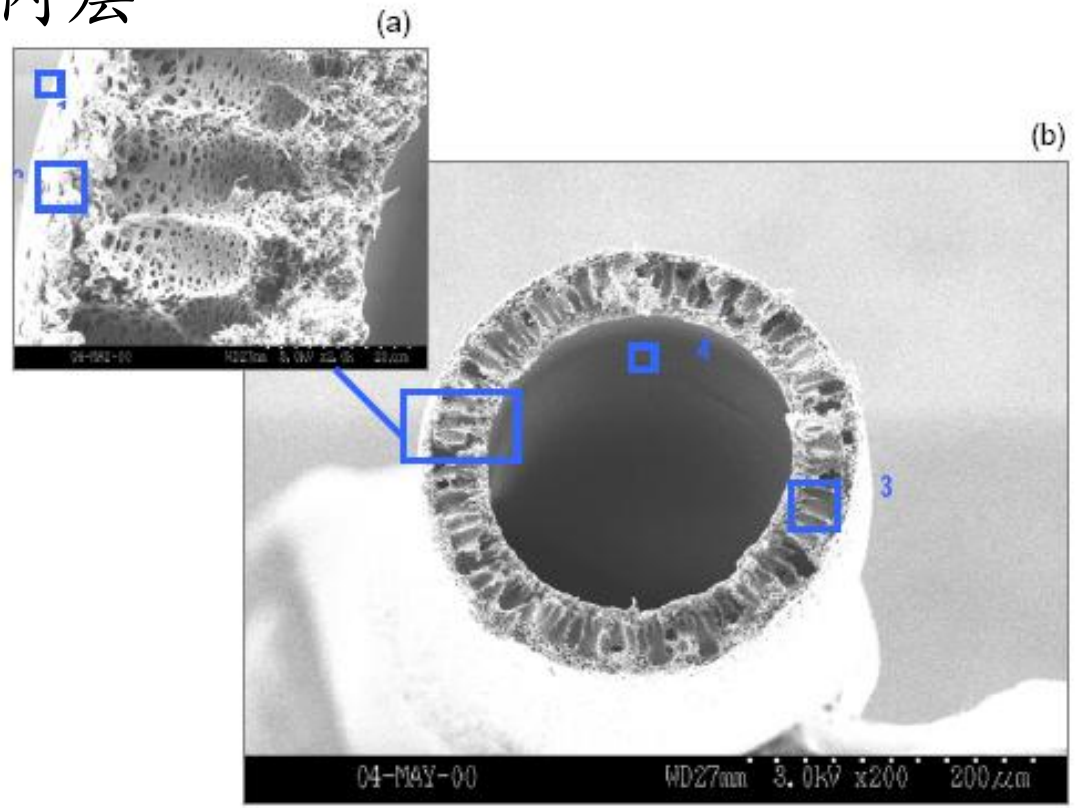

Figure 2.3 The scanning electron micrographs of a Polyflux 17S hollow fiber at (a) 2000X and (b) 200X. These micrographs show cross-sectional views of the unique morphology of the hollow fiber: (1) outer skin layer, (2) intermediate support layer, (3) finger-like structure layer, and (4) microdomain inner layer. The Polyflux 17S hollow fiber is made of Polyamide S™.

多孔介质的中空纤维
从内向外分布了三种孔径结构

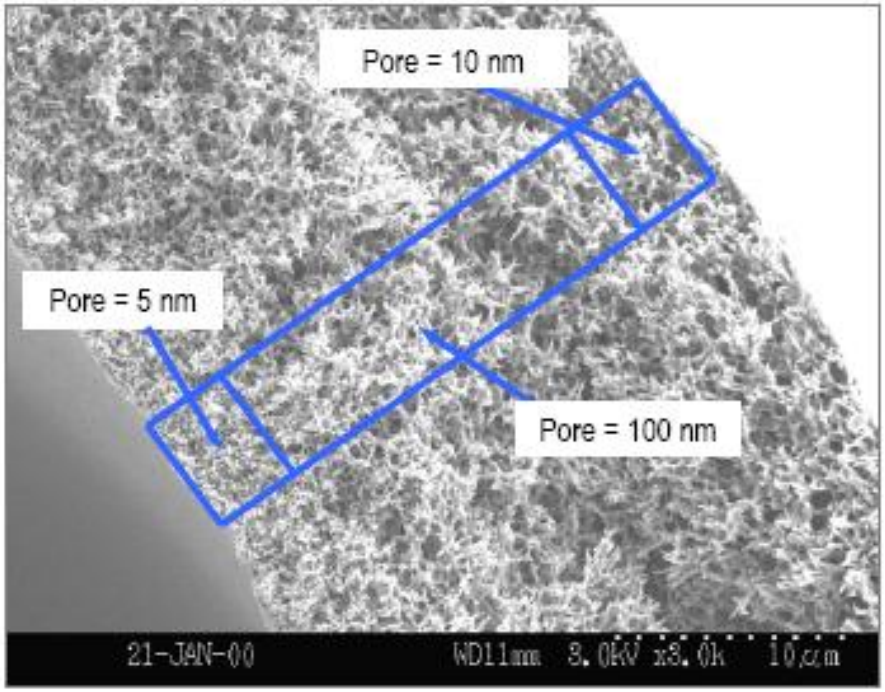

Figure 2.4 The scanning electron micrograph of a SYNTRA 160 hollow fiber at 8000X. This micrograph shows cross-sectional view of the three unique layers of the hollow fiber each with different average pore sizes. The outer skin, intermediate and inner skin layers have average pore sizes of 10, 100, and 5 nm respectively. The SYNTRA 160 hollow fiber is made of DIAPES®.

人工肾的传输

人工肾性能评价指标：由血液中去除的尿毒溶质的量决定

$$Kt/V$$

K　　尿素清除率

T　　血液透析时间

V　　病人尿素体积，约等于人总体的水量

通常

$Kt/V \geq 1.2$　病人能得到足够的透析

$Kt/V < 1.2$　透析不完整，有可能会增加死亡率

$Kt/V \geq 1.3$　不会进一步提高生存率

透析膜清除尿毒溶质的两大机理

- 扩散
- 对流

扩散传输

扩散传输的驱动力：　　透析膜内外的浓度差

扩散传输：从较高浓度的区域传至较低浓度的区域，是一种被动传输

血液流动部分和透析液部分存在浓度差，从而产生扩散。膜内外浓度差越大，传输速度越快

影响传输率的因素：溶质分子重量以及透析膜的几何特性：孔穴率和膜的厚度

经过透析膜的尿毒溶质传输率

$$J_{s,z} = -D_s \frac{dc}{dz}$$

Fick's Law

$J_{s,z}$ 溶质在扩散方向上的扩散摩尔流量mol/m^{2}s

D_s 经透析膜的溶质扩散系数 m^2/s

$\frac{dc}{dz}$ 膜透过方向的浓度梯度 mol/m^3/m

因此，溶质扩散传输率与 透过膜方向的浓度差成正比，与定温定压下的膜厚度成反比

负号：沿浓度减小的方向

溶质扩散系数与溶质分子的移动性 mobility有关

由Stokes-Eistein公式给出

$$D_s = \frac{\kappa T}{6\pi r_s \mu}$$

κ	波尔兹曼常数
μ	溶剂粘度
T	绝对温度
r_s	溶质的等效球半径或Stokes半径

$$D_s = \frac{RT}{6\pi r_s N_A} \qquad r_s = \frac{M_s}{4\pi\rho N_A}$$

R	气体常数
N_A	阿伏加德罗常数
M_s	溶质分子量
ρ	溶质的水合密度

影响溶质扩散系数的因素：温度，压力，粘度，溶液的溶质组成，分子大小，膜的物理化学特性

对于整个膜而言，它的物质传输率可表示为

$$Q_D = K_o A \Delta C$$

K_o　　溶质总的质量传输系数

ΔC　　透过膜的浓度差,由溶质的对数平均浓度差给出(与对流换热器中的对数平均温差相类似

$$\Delta C = \frac{(C_{bi} - C_{do}) - (C_{bo} - C_{di})}{\ln\left[\frac{C_{bi} - C_{do}}{C_{bo} - C_{di}}\right]}$$

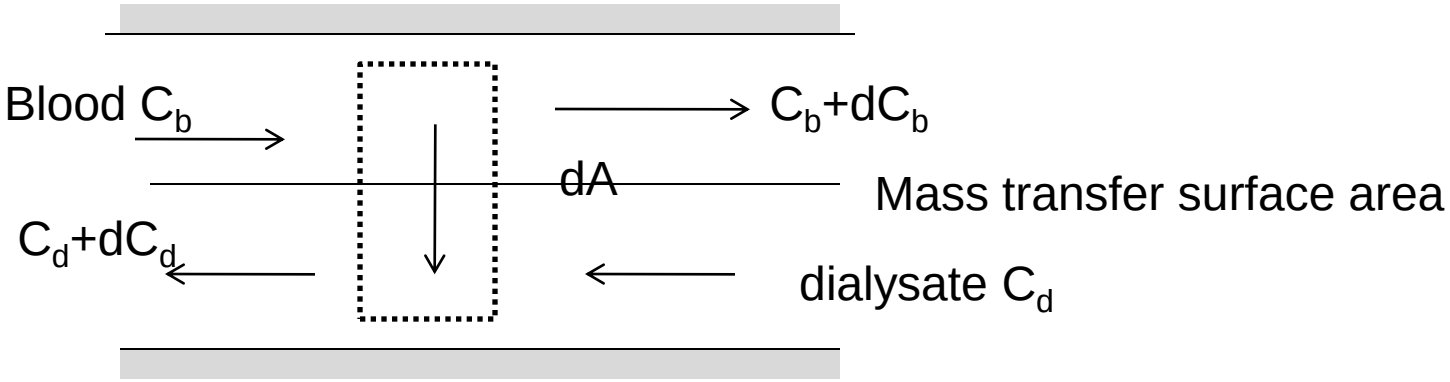
Blood C_b
C_b+dC_b
dA
Mass transfer surface area
C_d+dC_d
dialysate C_d

逆流传质装置浓度变化

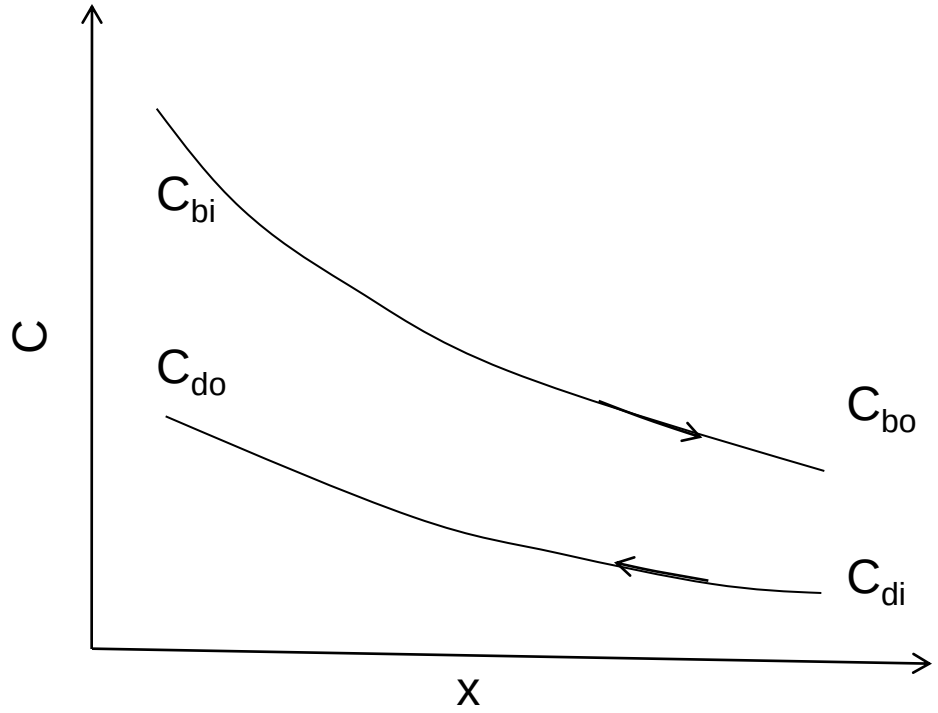
C
C_{bi}
C_{do}
C_{bo}
C_{di}
x

$$\frac{Q_d}{A} = \frac{\Delta C}{R_{oR}}$$

提高某一溶质的清除率的方法:

- 增加透过膜的浓度差
- 减少溶质的传质阻抗

$$R_{oR} = \frac{1}{K_o}$$

阻抗传质总传质系数的倒数

$$R_{oR} = R_B + R_M + R_D$$

总传质阻抗由血液测,膜内,以及透析液部分的阻抗组成

$$\frac{1}{K_o} = \frac{1}{k_B} + \frac{1}{P_s} + \frac{1}{k_D}$$

P_s 扩散溶质在膜内的透过率

溶质扩散清除率的定义：
在单一通道中溶质传质率与血液侧进口浓度之比。
通常在注入透析液时，不含所要透析的溶质，所以 $C_{di}=0$

$$Q_b(C_{bi}-C_{bo})=Q_d(C_{do}-C_{di})$$

溶质在血液侧的清除率

$$K_{b,diff}=\frac{Q_b(C_{bi}-C_{bo})}{C_{bi}}$$

溶质在透析液侧的清除率

$$K_{d,diff}=\frac{Q_d(C_{do}-C_{di})}{C_{bi}}$$

$$K_{b,diff}=K_{d,diff}$$

对流传输

由透过膜的压力差引起

$$Q_{uf} = K_{uf} \Delta P$$

Q_{uf}　　对流传质率

K_{uf}　　过滤系数

ΔP　　透过膜的压力差

在实际运行中，对流和扩散传输过程并存

➢对于低流量透析装置，

通过扩散过程清除低分子量的尿毒溶质

通过对流过程清除多余的等离子水

➢对于高流量透析装置，

通过扩散过程清除低分子量和中分子量的尿毒溶质

通过对流过程清除中分子量和高分子量的尿毒溶质以及多余的等离子水

横跨膜内的流动：Kedem-Katchalsky Equations (K-K Equations)

$$J_s = P_s \Delta C + (1-\sigma) J_v C_m$$

J_s 跨膜的净溶质流量

P_s 单位膜厚度透过率 （permeability）

ΔC 膜内外侧的浓度差

σ 溶质的Staverman 反射系数

J_v 透过膜的溶液体积流量

C_m 膜内溶质的平均浓度

$$C_m = (1-f)C_b + fC_d$$

$$f = \frac{1}{Pe} - \frac{1}{e^{Pe}-1} \qquad 0 \le f \le 1$$

表征对流传输和扩散传输之间的强弱 → $$Pe = \frac{(1-\sigma)J_v}{P_s}$$

溶液的体积流量 $m^3/m^2/s$

$$J_v = L_p(P_1 - P_2) - \sigma L_p RT(C_1 - C_2)$$

L_p 溶液经过透析膜的过滤系m/s/Pa

P_1, P_2 膜内外的流体压力

C_1, C_2 膜内外的溶质浓度

L_p, P_s, σ 膜的固有特性参数

模拟人工肾内的传质
传质过程包括三相 ：血液，膜，透析液

Step1： 血液中的溶质由于浓度差和径向对流，溶质会传输到膜表面 （血液侧）

Step2： 溶质由于在血液侧和透析液侧的浓度差和压力梯度，通过透析膜（膜内）

Step3： 溶质被从膜表面出去至透析液中（透析液侧）

Equivalent Annulus Model（等效环状模型）

- 血液侧和透析液侧的流体流动由Navier-Stokes方程求解
- 由K-K方程分析穿过膜的流量
- N-S方程为K-K方程提供膜内表面的溶液压力和浓度分布；K-K方程为N-S方程提供透过膜后的溶液流量和浓度

等效环状模型

$$R_e = \frac{R_m}{\sqrt{N}}$$

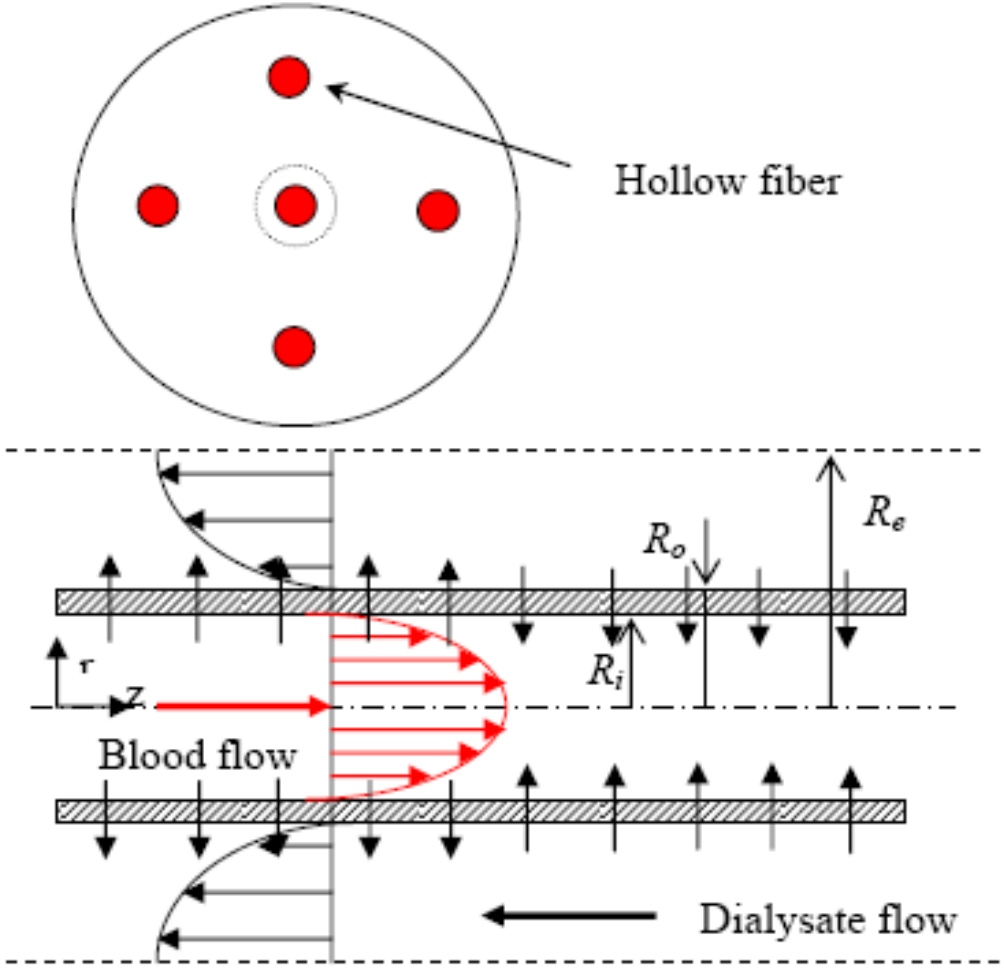

透过膜的传质过程

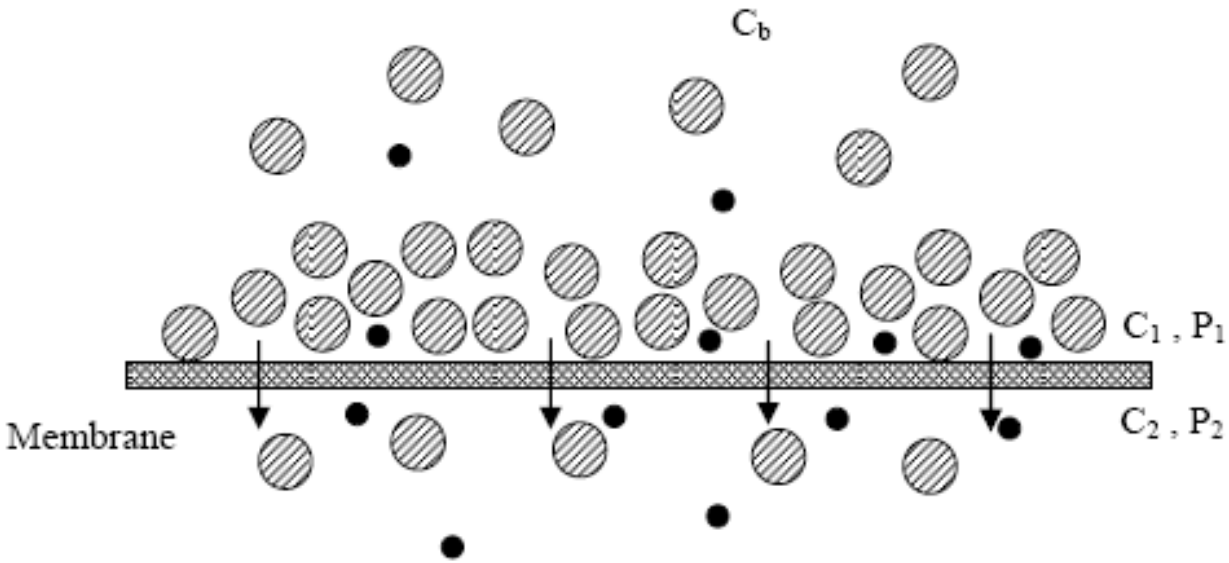

Figure 4.2 Mass transport through membrane

膜内传质过程

K-K 方程

对于多重结构的跨膜溶质通量可以表示为

$$J_s = \frac{J_v S_{\infty 1} S_{\infty 2} S_{\infty 3} (\alpha_1 \alpha_2 \alpha_3 C_{Bs} - C_{Ds})}{S_{\infty 1} S_{\infty 2} (\alpha_3 - 1) + S_{\infty 1} S_{\infty 3} (\alpha_2 - 1)\, \alpha_3 + S_{\infty 2} S_{\infty 3} (\alpha_1 - 1)\, \alpha_2 \alpha_3}$$

$S_{\infty i}$ 区域i的过滤系数

$\alpha_i = \left(\frac{R_{i+1}}{R_i} \right)^{Pe_i}$ 区域i内对流和扩散的重要度比

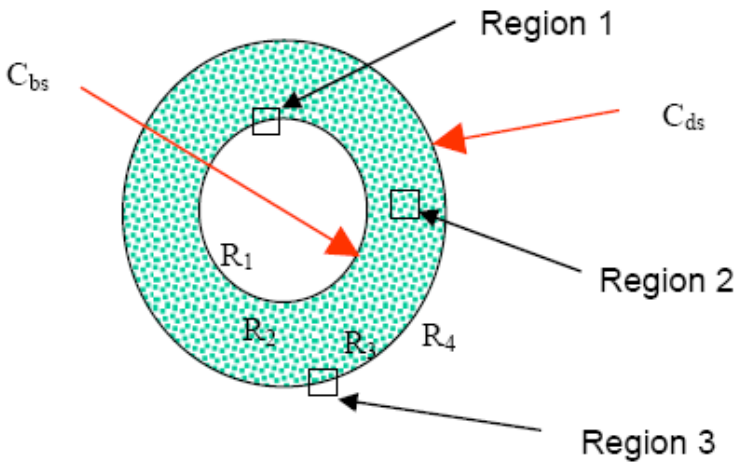

Figure 4.3 Three regions of dual-skinned hollow-fiber membrane: inner skin (region 1), porous matrix (region 2), outer skin (region 3)

血液流动的控制方程

Continuity equation:

$$\nabla \cdot \mathbf{u}_b = 0 \tag{4.2}$$

Momentum equations:

$$\rho_b(\mathbf{u}_b \cdot \nabla \mathbf{u}_b) = -\nabla P_b + \mu_b \nabla^2 \mathbf{u}_b \tag{4.3}$$

Concentration equation:

$$\mathbf{u}_b \cdot \nabla C_b = D\ \nabla^2 C_b \tag{4.4}$$

透析液流动的控制方程

Continuity equation:

$$\nabla \cdot \mathbf{u}_d = 0 \tag{4.5}$$

Momentum equations:

$$\rho_d(\mathbf{u}_d \cdot \nabla \mathbf{u}_d) = -\nabla p_d + \mu_d \nabla^2 \mathbf{u}_d \tag{4.6}$$

Concentration equation:

$$\mathbf{u}_d \cdot \nabla C_d = D\ \nabla^2 C_d \tag{4.7}$$

膜内传质过程和流动过程的耦合

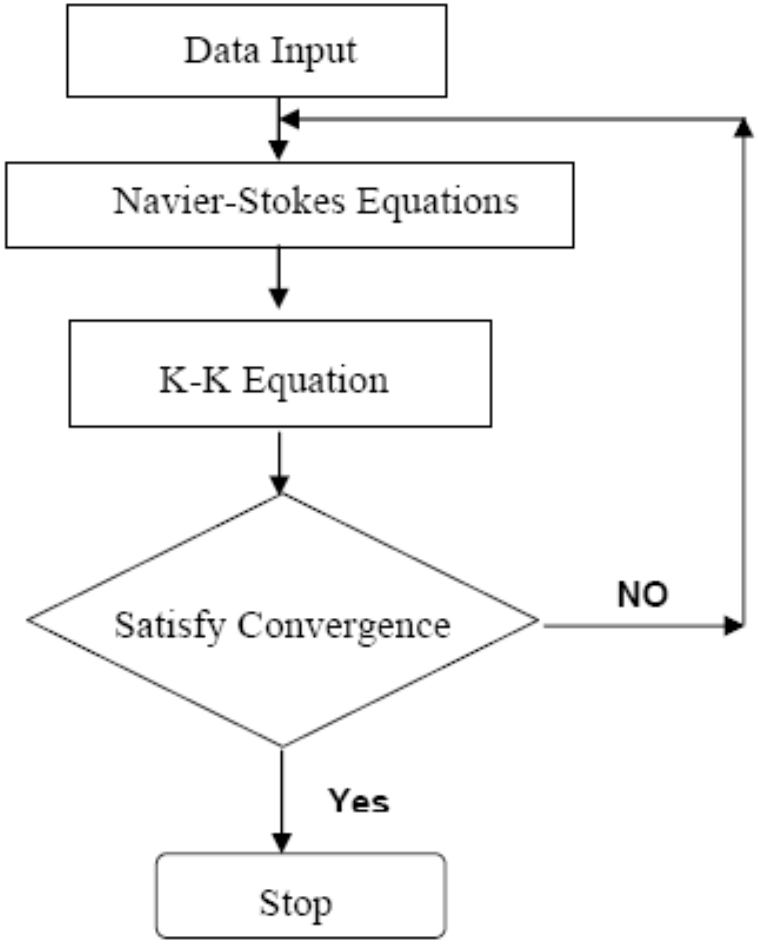

Figure 4.4 Flow chart of computer algorithm

不同透析器的物性参数

Table 4.2 Effective transport properties of membrane in CT190G and PolyFlux 17s

		CT190G	PolyFlux 17s
Hydraulic permeability L_p^* (m/s/Pa)		3.95×10^{-11}	2.30×10^{-10}
Diffusive permeability P_s^* (m/s)	urea	2.80×10^{-5}	2.30×10^{-5}
	creatinine	1.57×10^{-5}	1.33×10^{-5}

透析器滤除率的计算结果与实验结果的比较

Table 4.3 Comparison of Clearance by a new algorithm in CT190G

Q_{bi} (ml/min)	Q_{di} (ml/min)	Clearance of urea (ml/min)			Clearance of creatinine (ml/min)		
		Exp.	Num.	Error	Exp.	Num.	Error
300	200	195.56	189.76	2.97%	185.98	180.42	2.99%
300	300	234.83	223.21	4.95%	215.82	205.20	4.92%
300	400	266.56	265.20	0.51%	248.12	246.05	0.83%
400	200	212.34	212.33	0.00%	207.31	203.97	1.61%
400	400	294.49	292.57	0.65%	262.58	262.48	0.04%
400	500	305.62	313.73	2.65%	274.14	278.85	1.72%

血液出口处的尿素浓度比较

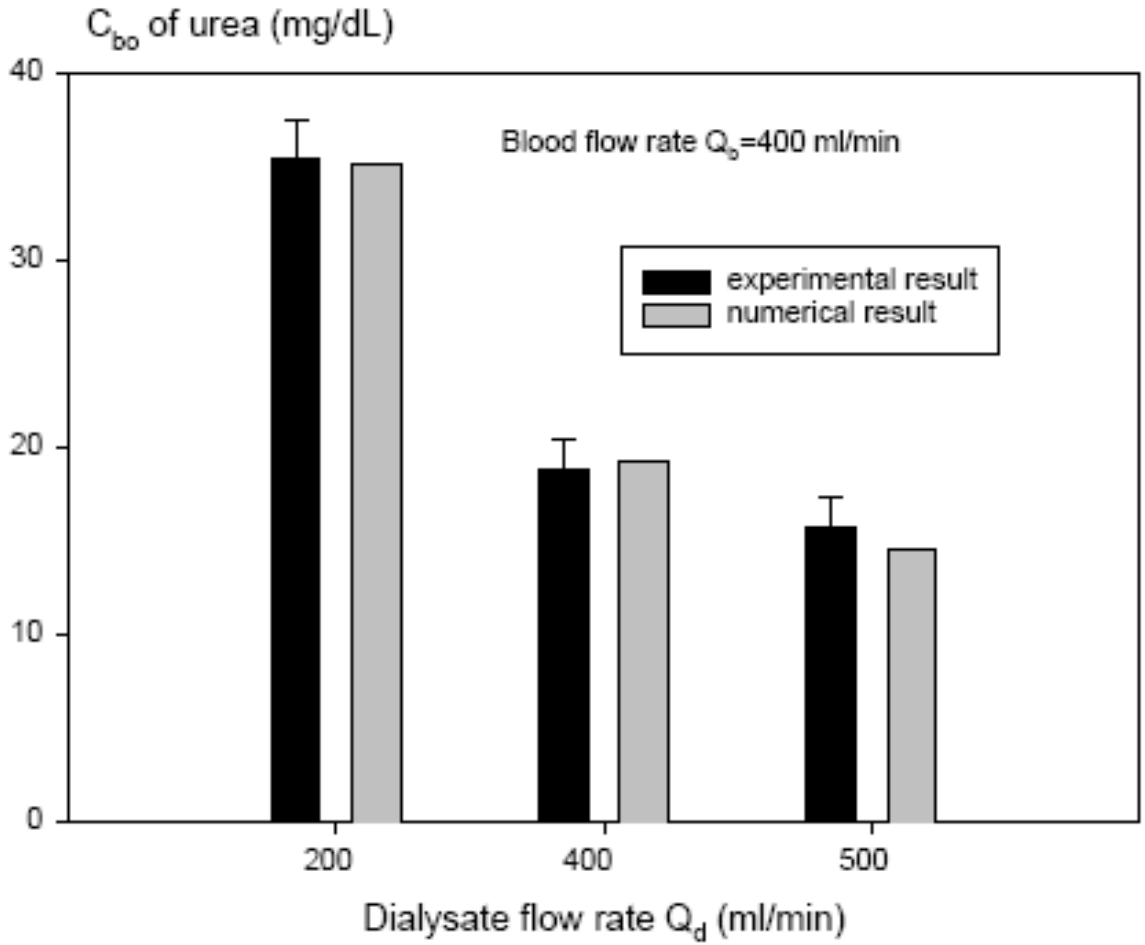

Figure 4.5 Concentration of urea in the outlet of blood flow (n=3)

尿素分别在血液侧和出口侧的径向分布

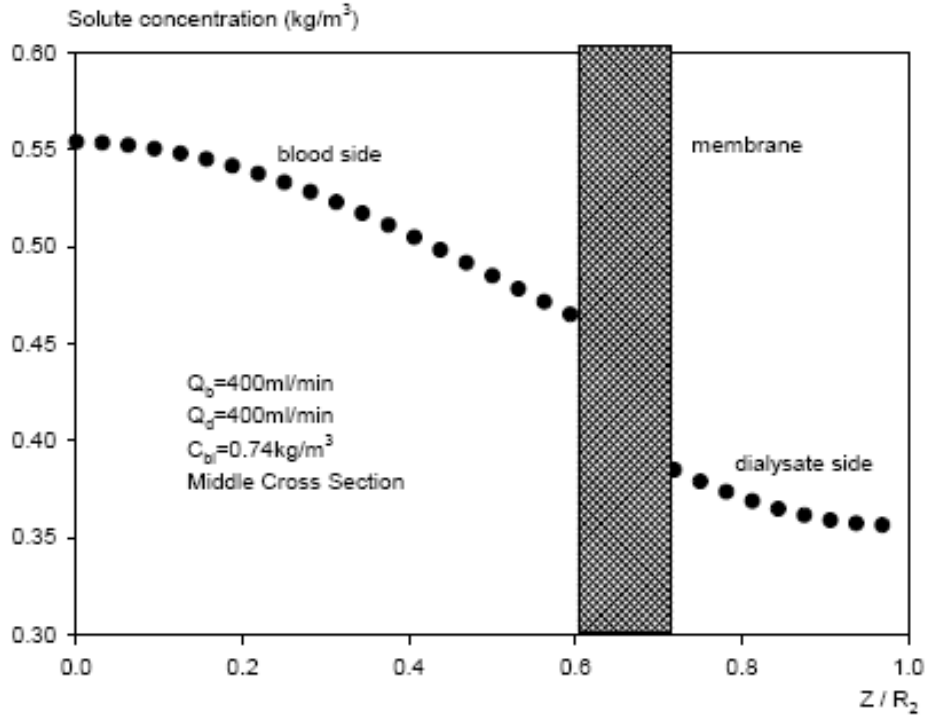

Figure 4.7 Radial distribution of urea concentration in blood and dialysate side

(Dialyzer: CT190G; Membrane: Cellulose Triacetate; Location: Middle cross section;

L_p =1.15×10-10 m/s/Pa; P_s=9.76×10-6 m/s)

血流量一定，透析液浓度不同时血液出口处的尿素浓度

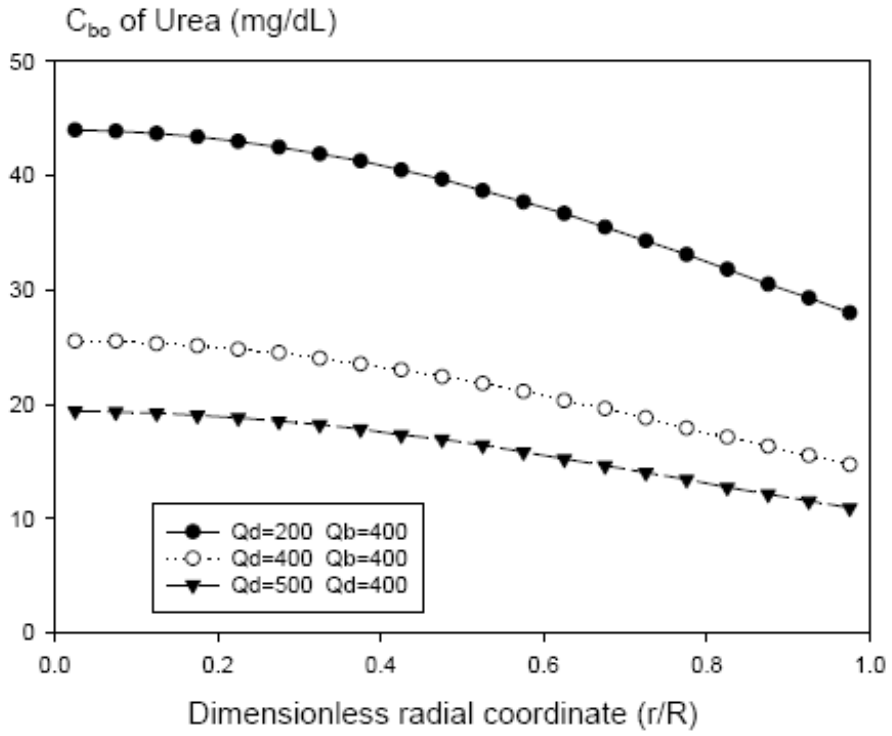

Figure 4.8 Radial distribution of urea concentration under different blood rates

(Dialyzer: CT190G; Membrane: Cellulose Triacetate; Location: Middle cross section;

轴向方向上经膜的渗透速度分布

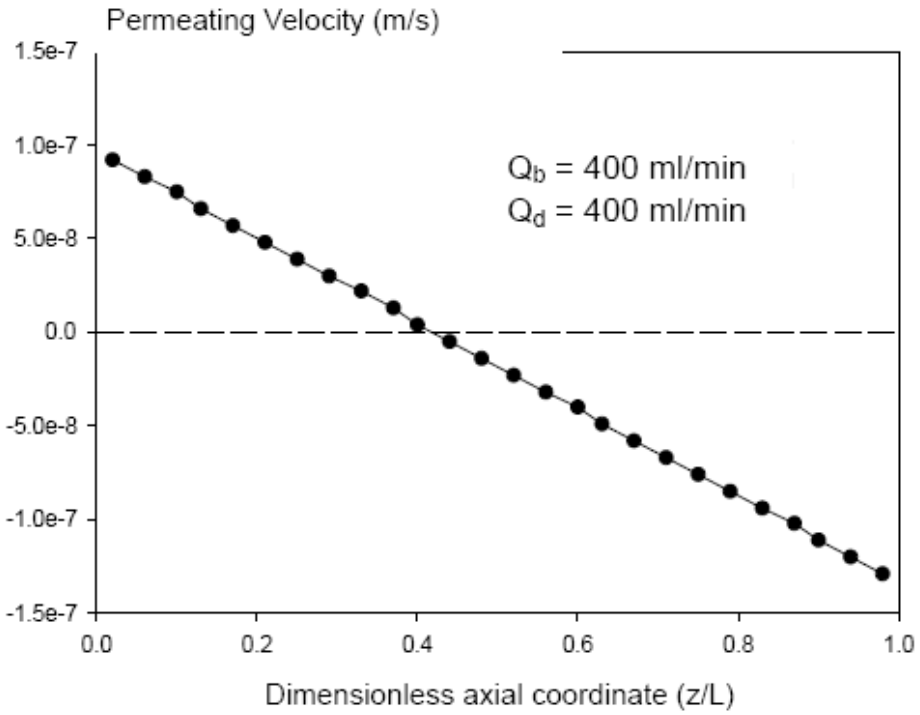

L_p= 1.15×10-10 m/s/Pa; P_s=9.76×10-6 m/s)

Figure 4.10 Axial distribution of permeating velocity (Dialyzer: CT190G; Membrane: Cellulose Triacetate; L_p=1.15×10-10 m/s/Pa; P_s=9.76×10-6 m/s)

轴向方向上经膜的渗透压力分布

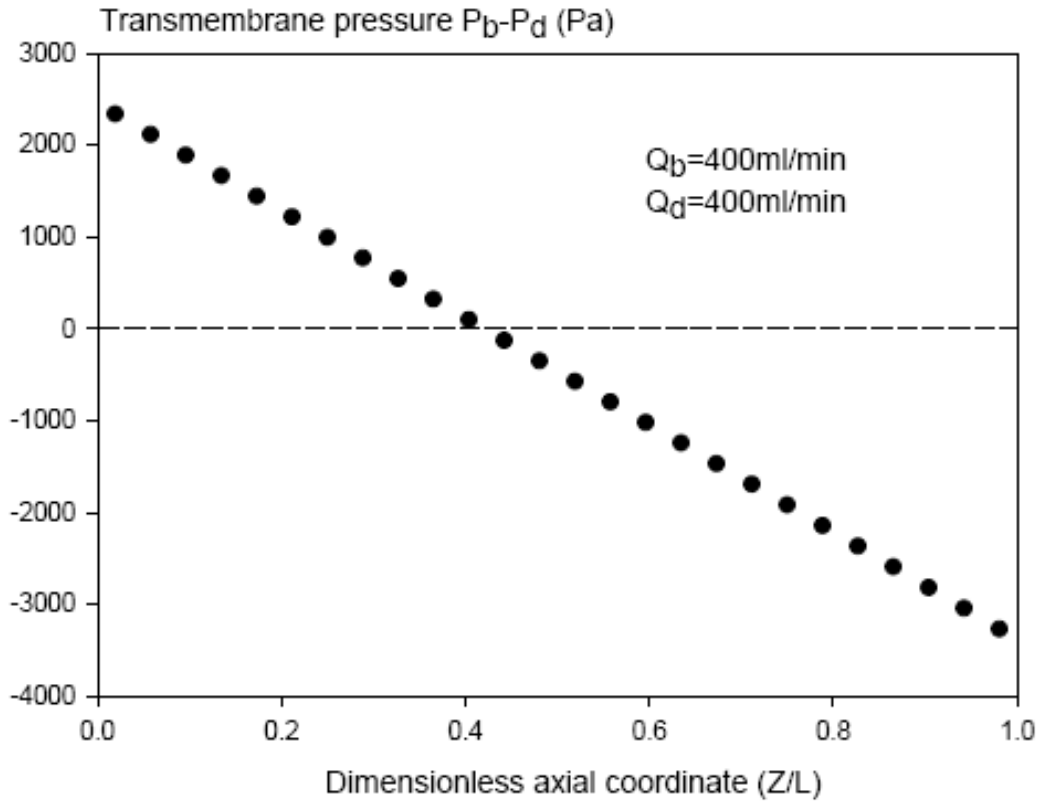

Figure 4.11 Axial distribution of transmembrane pressure (Dialyzer: CT190G; Membrane: Cellulose Triacetate; L_p=1.15×10^{-10} m/s/Pa; P_s=9.76×10^{-6} m/s)

新型薄膜洗肾仪器,
生物工程与纳米科技研究院（新加坡)研制

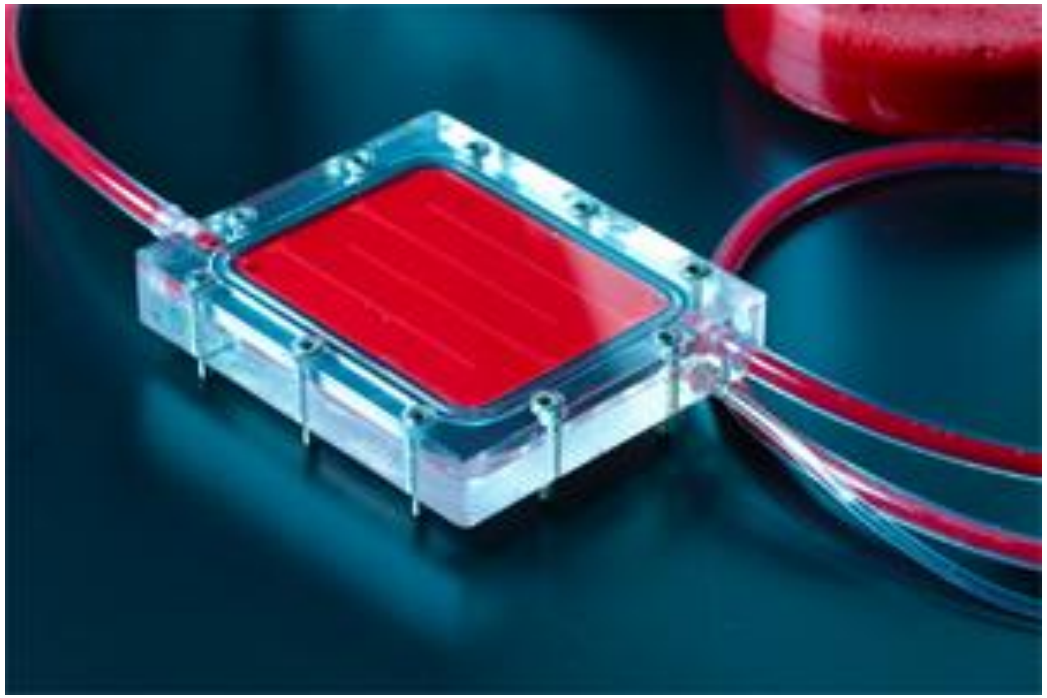

透析液流动在透析装置中流动的多孔介质模型

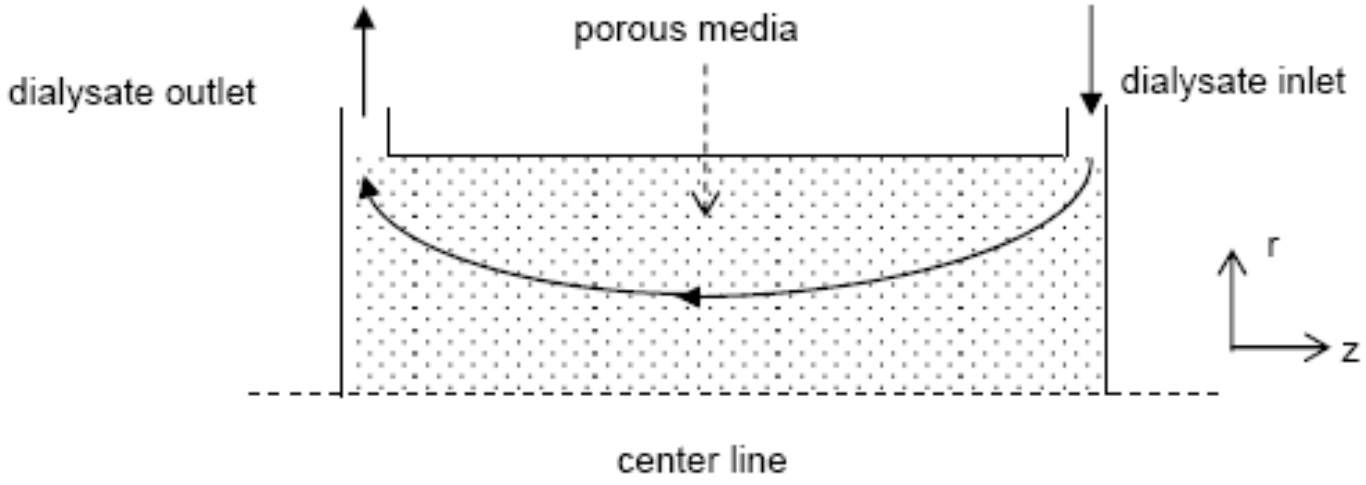

Figure 5.2 Two-dimensional dialysate flow pattern

透析液侧的连续，动量以及浓度方程

$$\nabla \cdot \mathbf{u_d} = -S_m$$

$$u_{r,d} = -\frac{k_{rr,d}}{\mu_d}\frac{\partial p_d}{\partial r}$$

$$u_{z,d} = -\frac{k_{zz,d}}{\mu_d}\frac{\partial p_d}{\partial z}$$

$$\mathbf{u_d} \cdot \nabla C_d = S_s$$

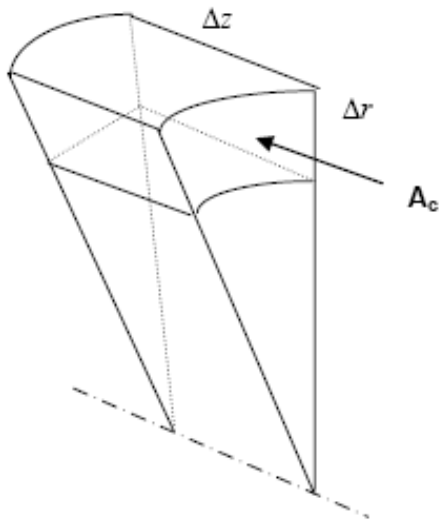

Figure 5.3 Fluid control volume

$$S_m = \frac{J_v \cdot A_m}{A_c \cdot \Delta z}$$

$$S_s = \frac{J_s \cdot A_m}{A_c \cdot \Delta z}$$

多孔介质模型的计算流程图

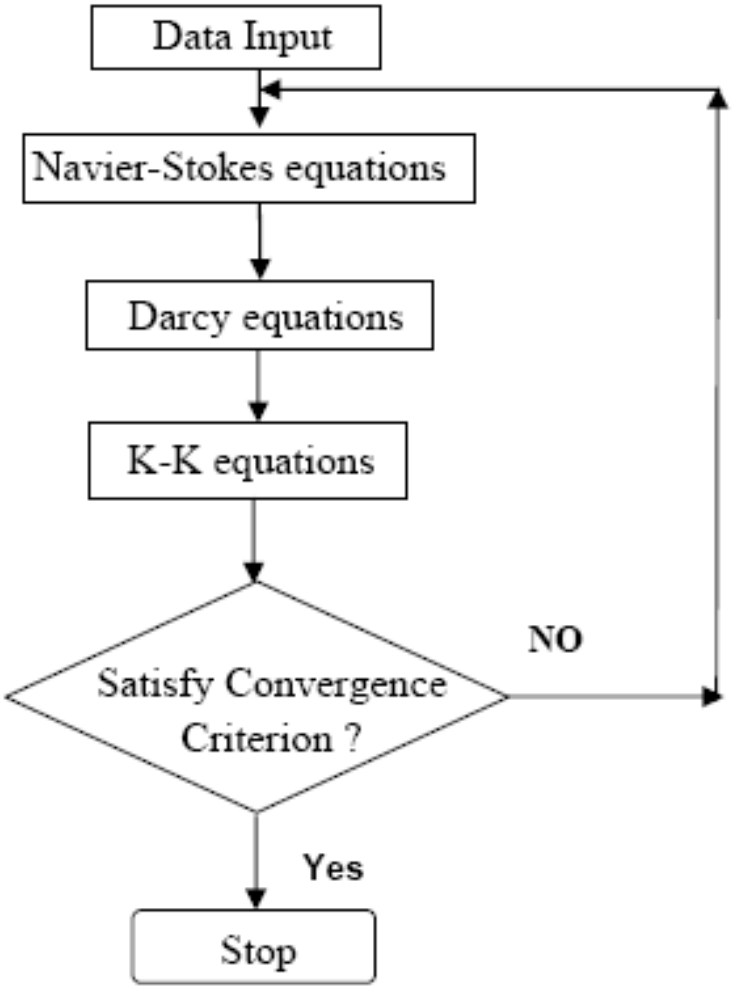

Figure 5.4 Flow chart of computer algorithm

透析液流量变化时对应的进出口压力变化

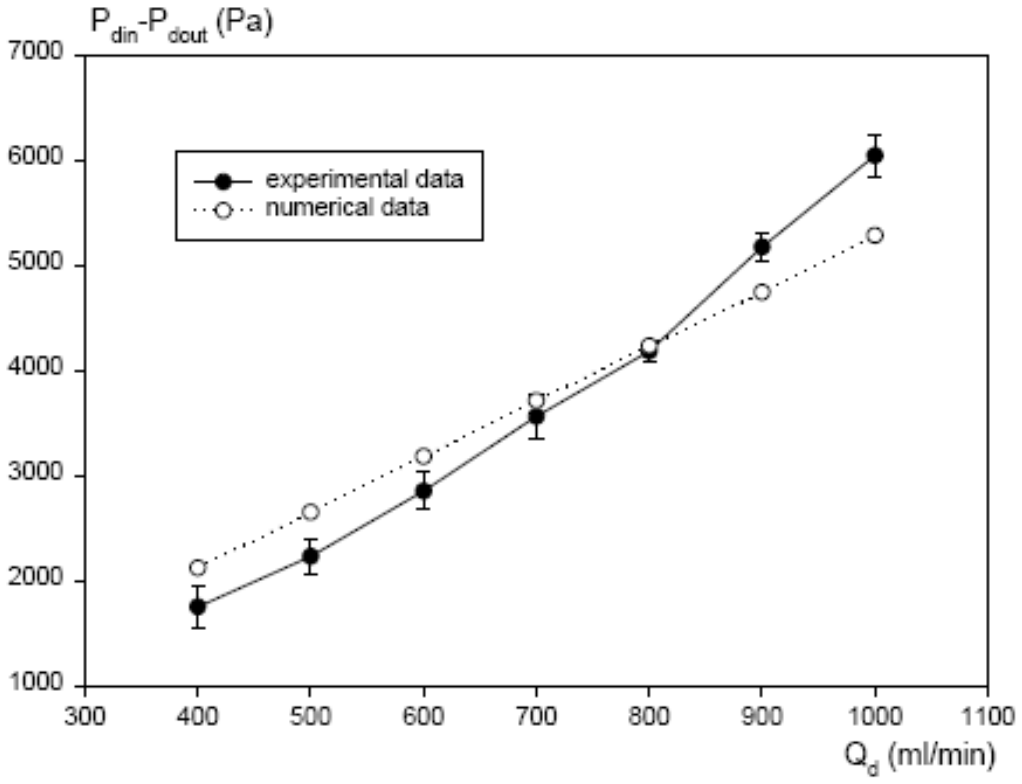

Figure 5.5 Pressure loss between dialysate inlet and outlet (n=3)

透析液在透析装置内尿素的浓度变化

血液和透析液的流量以及尿素的浓度

Q_b=360ml/min, Q_d=500ml/min, C_b=48.0mg/dL

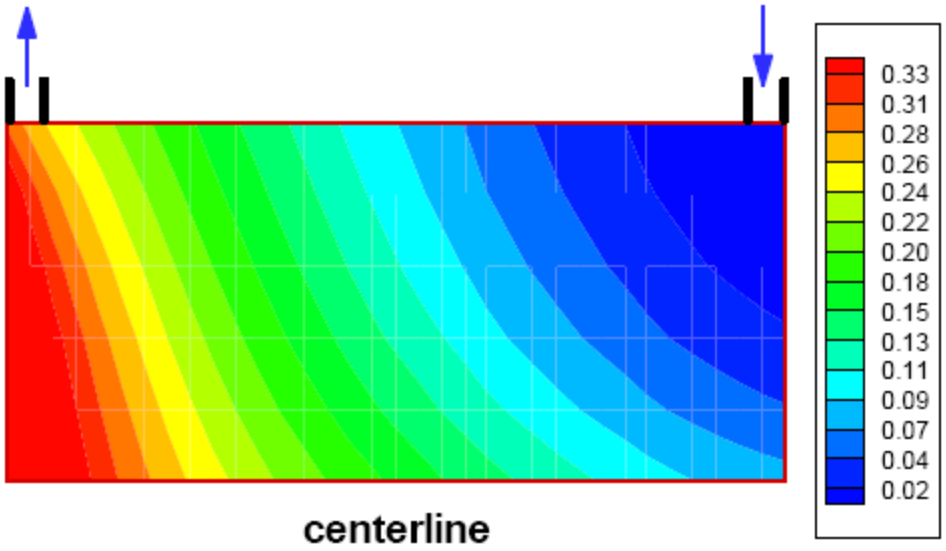

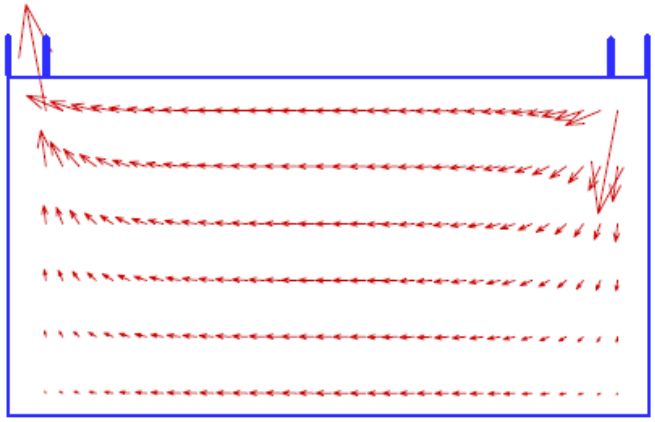

Figure 5.6 Velocity field in dialysate side

对于CT190G的透析装置
透析液的速度分布

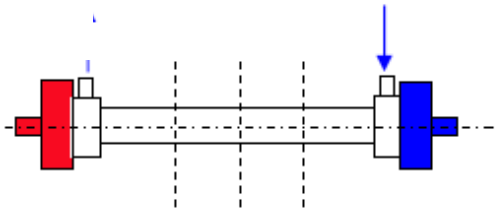

(1) (2) (3)

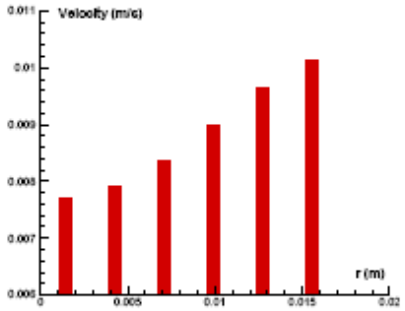

(1)

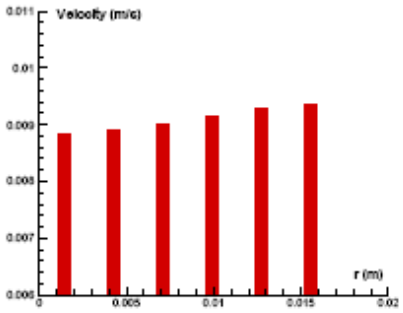

(2)

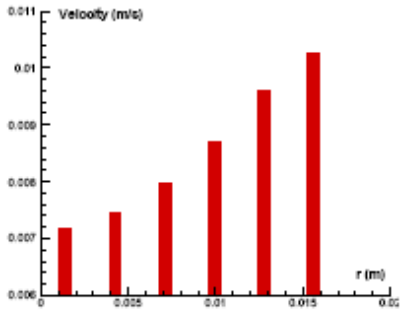

(3)